Tetrahedron 65 (2009) 8336–8343

Contents lists available at ScienceDirect

Tetrahedron

journal homepage: www.elsevier.com/locate/tet

Photophysical properties of phenanthro[9,10-*d*]imidazole-type fluorescent hosts upon inclusion of organic solvent molecules

Yousuke Ooyama *, Hironori Kumaoka, Kazuki Uwada, Katsuhira Yoshida *

Department of Material Science, Faculty of Science, Kochi University, Akebono-cho, Kochi 780-8520, Japan

ARTICLE INFO

Article history:
Received 23 July 2009
Received in revised form 10 August 2009
Accepted 11 August 2009
Available online 14 August 2009

Keywords:
Solid-state fluorescence
Fluorescent clathrate
Crystal structures
Dyes
Optical property

ABSTRACT

The crystal of phenanthro[9,10-*d*]imidazole-type fluorescent clathrate host (**1**) exhibits fluorescence enhancement behavior with a blue-shift of the emission maximum upon enclathration of organic solvent molecules such as 1-butanol and morpholine, whereas the crystal of **1** exhibits fluorescence enhancement behavior with a red-shift of the emission maximum upon enclathration of carboxylic acid such as acetic acid and propionic acid. The crystal structures of the guest-free and the guest-inclusion compounds of **1** have been determined by X-ray analysis. On the bases of the spectral data and the crystal structures, the effects of the enclathrated guest molecule on the solid-state photophysical properties of the guest-inclusion compounds are discussed.

1. Introduction

Organic fluorescent hosts, which exhibit sensitive color and fluorescence intensity changes upon formation of host/guest-inclusion complexes in the crystalline state, can be one of the most promising materials for the construction of desirable solid-state fluorescent system.[1–4] Some groups have reported that the crystal of fluorescent host exhibits fluorescence enhancement behavior upon enclathration of organic solvent molecules. The fluorescence enhancement is greatly dependent on the identity of the enclathrated guest molecules. From the comparison of the X-ray crystal structures of the guest-free and several clathrate compounds, it was concluded that the destructions of the π–π interactions or continuous intermolecular hydrogen bonding between fluorescent hosts by the enclathrated guest molecules are the main reason for the guest-dependent fluorescence enhancement of the crystals.[2–4] As the results, the improvement of solid-state fluorescence intensity has been achieved. However, the modulation of solid-state fluorescence wavelength controlled by enclathrated guest is not yet successfully established.

For the purpose of controlling solid-state fluorescence wavelength by clathrate formation, we have designed and synthesized a phenanthro[9,10-*d*]imidazole-type fluorescent clathrate host, 2-[4-(diphenylamino)phenyl]-1*H*-phenanthro[9,10-*d*]imidazole (**1**) with imidazole ring and diphenylamino group (Scheme 1). We found that the crystal of **1** exhibits fluorescence enhancement behavior with a blue-shift of the emission maximum upon enclathration of organic solvent molecules such as 1-butanol and morpholine, whereas the crystal of **1** exhibits fluorescence enhancement behavior with a red shift of the emission maximum upon enclathration of carboxylic acid such as acetic acid and propionic acid. Our results indicated that the modulation of the solid-state fluorescence properties should be achieved by a combination of the fluorescent clathrate host and guest molecule. In this paper, on the bases of the spectral data and the X-ray crystal structures of guest-inclusion compounds, the effects of the enclathrated guest molecules on the solid-state photophysical properties of the clathrate compounds are discussed.

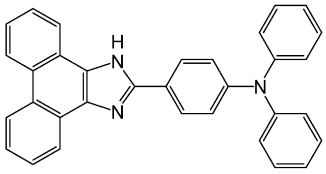

1

Scheme 1. Chemical structure of the phenanthro[9,10-*d*]imidazole-type fluorescent clathrate host (**1**).

* Corresponding authors. Tel.: +81 88 844 8296; fax: +81 88 844 8359.
E-mail addresses: yooyama@hiroshima-u.ac.jp (Y. Ooyama), kyoshida@cc.kochi-u.ac.jp (K. Yoshida).

0040-4020/$ – see front matter © 2009 Elsevier Ltd. All rights reserved.
doi:10.1016/j.tet.2009.08.027

2. Results and discussion

2.1. Spectroscopic properties of 1 in solution

The absorption and fluorescence spectra of **1** in 1,4-dioxane, ethanol, 1-butanol, morpholine, and acetic acid are shown in Figure 1, and the absorption and fluorescence spectral data summarized in Table 1. The fluorophore **1** exhibits an absorption band at around 365 nm with a shoulder at around 380 nm in both 1,4-dioxane and morpholine. The corresponding fluorescence band was observed at 401 nm with a shoulder at 417 nm in 1,4-dioxane and at 419 nm in morpholine. On the other hand, in both ethanol and 1-butanol the fluorophore **1** exhibits an absorption band at around 365 nm with a shoulder at 373 nm and a fluorescence band at around 417 nm. Interestingly, in acetic acid, the absorption band of **1** appeared at around 384 nm, which was red-shifted by 19 nm compared with that observed in 1,4-dioxane. The corresponding fluorescence maximum was observed at around 502 nm, which was red-shifted by 101 nm compared with that in 1,4-dioxane. The absorption and fluorescence maxima of 2-(4′-(*N*,*N*-dimethylamino)phenyl)benzimidazole in acidic solution were red-shifted compared with that in neutral solution, which has been reported by Dogra et al.[5] It was elucidated that the red-shifts are induced by the protonation to an imino nitrogen atom of imidazole ring. In our case, it was considered that the observed red-shifts of **1** in acetic acid are caused by the protonation to an imino nitrogen atom of imidazole ring, as shown in Scheme 2. The fluorescence quantum yield (Φ) of **1** in 1,4-dioxane, ethanol, 1-butanol, morpholine, and acetic acid are 0.73, 0.82, 0.80, 0.52, and 0.32, respectively.

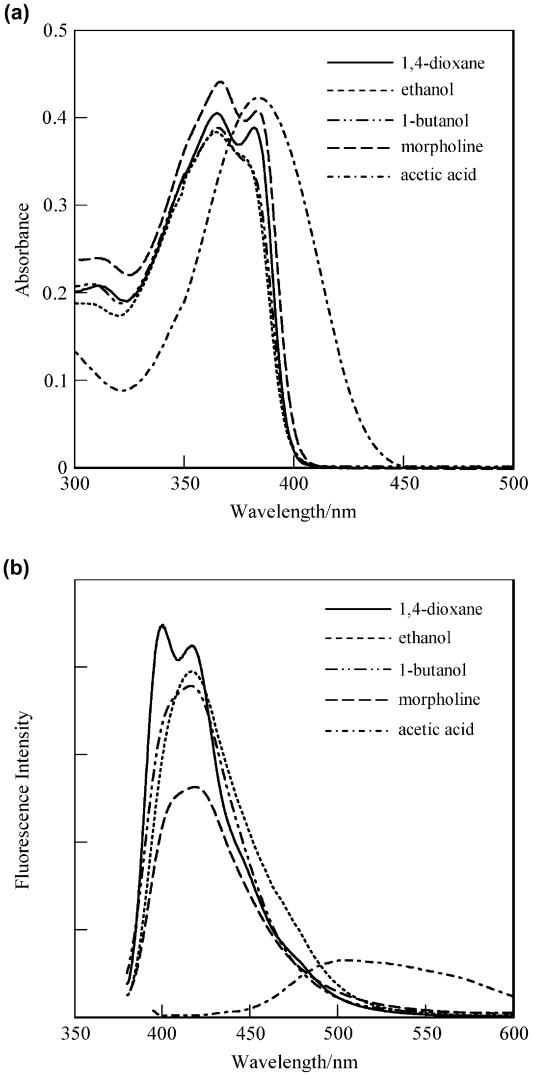

Figure 1. (a) Absorption and (b) fluorescence spectra of **1** in 1,4-dioxane, ethanol, 1-butanol, morpholine, and acetic acid.

Table 1
Spectroscopic properties of **1** in solution

Solvent	λ_{max}^{abs}/nm[a] [ε_{max}/dm^3 mol^{-1} cm^{-1}]	λ_{max}^{fl}/nm[b]	Φ[c]	SS[d] $\Delta\lambda_{max}$
1,4-Dioxane	365 (40,500), 381 (38,700)^{sh}	401, 417^{sh}	0.73	36
Ethanol	365 (38,300), 373 (36,300)^{sh}	417	0.82	52
1-Butanol	366 (38,700), 373 (36,400)^{sh}	416	0.80	50
Morpholine	367 (44,100), 383 (40,700)^{sh}	419	0.52	52
Acetic acid	384 (42,300)	502	0.32	118

[a] 1.0×10^{-5} M.
[b] 1.0×10^{-6} M.
[c] The Φ values were determined by using a calibrated integrating sphere system (λ_{ex}=363 nm).
[d] Stokes shift value.

2.2. Semi-empirical MO calculations (AM1, CNDO/S)

In order to understand the photophysical properties of 2-[4-(diphenylamino)phenyl]-1*H*-phenanthro[9,10-*d*]imidazole (**1**), we have carried out semi-empirical molecular orbital (MO) calculations of **1** by the CNDO/S method[6] after geometrical optimizations MOPAC/AM1 method.[7] Furthermore, we estimated the photophysical properties for **1**H$^+$ with the protonated imidazole ring, because it was assumed that the imino nitrogen atom of imidazole ring is protonated in acidic solution. The optimized geometry of **1** shows that the bond lengths between two nitrogens (N-1 and N-2) and C-2 in imidazole ring are 1.36 Å and 1.41 Å, respectively (Fig. 2). This result shows that the differences between the two lengths for **1** are attributed to the C–N single bond and the C=N double bond of imidazole ring. On the other hand, the two bond lengths for **1**H$^+$ are both 1.39 Å, which reveals the contribution of the resonance structure **1**H$^+$(**I**) as shown in Scheme 2. The bond lengths between C-3 of phenyl group and C-2 in imidazole ring are 1.46 Å for **1** and 1.44 Å for **1**H$^+$, and the bond lengths between C-1 of phenyl group and the nitrogen atom (N-3) of diphenylamino group are 1.41 Å for **1** and 1.38 Å for **1**H$^+$. The two bond lengths of **1**H$^+$ are shorter than those of **1**, which indicates the contribution of the resonance structure **1**H$^+$(**II**) (Scheme 1). The calculated absorption wavelengths and the nature of the transition of the absorption bands are summarized in Table 2. The calculated absorption wavelengths and the oscillator strength values of **1** and **1**H$^+$ are comparable with the observed spectra in 1,4-dioxane and acetic acid, respectively; the calculated absorption wavelength of **1**H$^+$ is shifted to longer wavelength compared to that of **1**, which is in good agreement with the experimental data in 1,4-dioxane and acetic acid. Therefore, the red-shift of **1** in acetic acid was explained by strong resonance interaction of the diphenylamino group with the protonated imidazole ring, leading to the resonance hybrid of **1**H$^+$(**I**) and **1**H$^+$(**II**).

2.3. Preparation of guest-inclusion crystals

The guest-free crystal of **1** was obtained by recrystallization of it from acetonitrile. The preparation of guest-inclusion crystals was attempted by recrystallization from the respective guest–solvent or guest-containing solvents. We have found that the host **1** yields inclusion compounds in stoichiometric ratios with acetic acid, propionic acid, 1-butanol, and morpholine. Interestingly, the

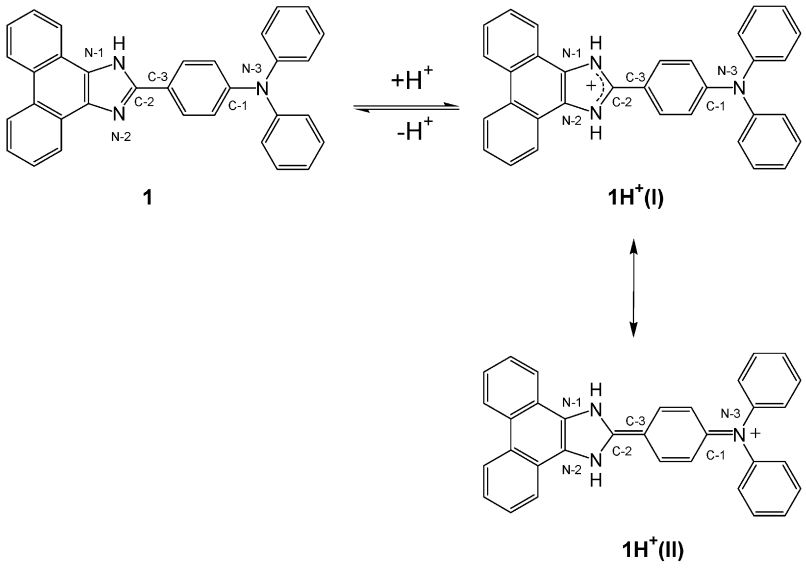

Scheme 2.

host **1** formed inclusion crystals with both morpholine and water by recrystallization from a mixture of morpholine and water. The characteristics of the guest-free and various guest-inclusion crystals obtained by co-crystallization of **1** from various solutions are summarized in Table 3. Compared to milk-white of the guest-free crystal, the color of the guest-inclusion crystals varied from white to yellow and a dramatic fluorescence enhancement was observed.

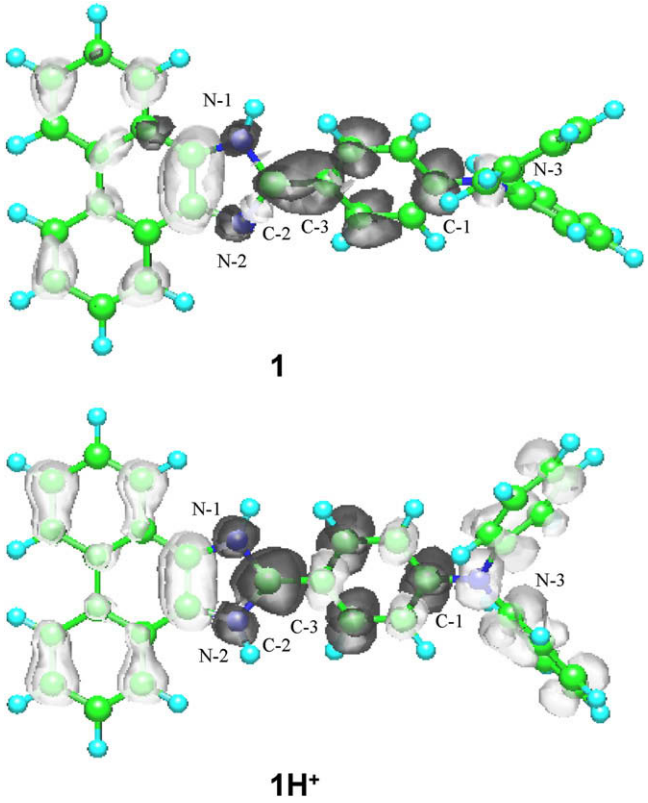

Figure 2. Calculated electron density changes accompanying the first electronic excitation of **1** and $\mathbf{1}H^+$. The black and white lobes signify decrease and increase in electron density accompanying the electronic transition. Their areas indicate the magnitude of the electron density change.

Table 2
Calculated absorption spectra for **1** and $\mathbf{1}H^+$

Species	μ/D[a]	Absorption (calcd)		CI component[c]	$\Delta\mu$/D[d]
		λ_{max}/nm	f[b]		
1	4.28	373	0.82	HOMO→LUMO (77%)	2.98
$\mathbf{1}H^+$	4.49	452	0.85	HOMO→LUMO (85%)	4.68

[a] The values of the dipole moment in the ground state.
[b] Oscillator strength.
[c] The transition is shown by an arrow from one orbital to another, followed by its percentage CI (configuration interaction) component.
[d] The values of the difference in the dipole moment between the excited and the ground states.

Table 3
Host–guest molar ratio, crystal form, and crystal color of the guest-free and the guest-inclusion crystals of **1**

Host	Guest	Host/guest (molar ratio)	Crystal form	Crystal color
1	None	1:0	Needle	Milk-white
	Acetic acid	1:1	Prism	Yellow
	Propionic acid	1:2	Prism	Yellow
	1-Butanol	1:1	Prism	Yellowish white
	Morpholine	2:1:2H_2O	Prism	White

2.4. Solid-state fluorescence change upon formation of guest-inclusion crystals

In order to investigate the effect of clathrate formation on the solid-state photophysical properties, the fluorescence excitation and emission spectra of the guest-free and the guest-inclusion crystals were measured (Fig. 3). The solid-state photophysical changes are greatly dependent on the identity of the enclathrated guest molecules. Compared to the guest-free crystal, the excitation and emission maxima of the 1-butanol- and morpholine-inclusion crystals exhibit a blue-shift, whereas those of acetic acid- and propionic acid-inclusion crystals exhibit a red shift. The fluorescence intensities of all the guest-inclusion crystals are enhanced to various degrees depending on the identity of the enclathrated guest molecules. The 416 nm band observed in the excitation spectrum of the guest-free crystals is blue-shifted to 413 nm and 398 nm in those of the 1-butanol- and morpholine-inclusion crystals, respectively, or red-shifted to 447 nm and 440 nm in those of the acetic acid- and propionic acid-inclusion crystals, respectively. The guest-free host crystal exhibits relatively weak fluorescence with emission maximum at 460 nm,

while the guest-inclusion crystals exhibit much stronger fluorescence intensity with the blue-shift of emission maximum to 459 nm and 432 nm in those of the 1-butanol- and morpholine-inclusion crystals, respectively, or the red-shift of emission maximum to 483 nm and 469 nm in those of the acetic acid- and propionic acid-inclusion crystals, respectively. Relative fluorescence intensity (RFI), which was determined by considering the fluorescence intensity of crystal **1** as 1.0, increases in the following order: **1**·acetic acid (RFI=1.1)<**1**·1-butanol (RFI=2.7)<**1**·morpholine (RFI=3.0)<**1**·propionic acid (RFI=4.6). These results indicate that the solid-state photophysical changes upon enclathration of guest molecules reflect strictly the changes in molecular packing induced by the enclathrated guest molecules in the crystals.

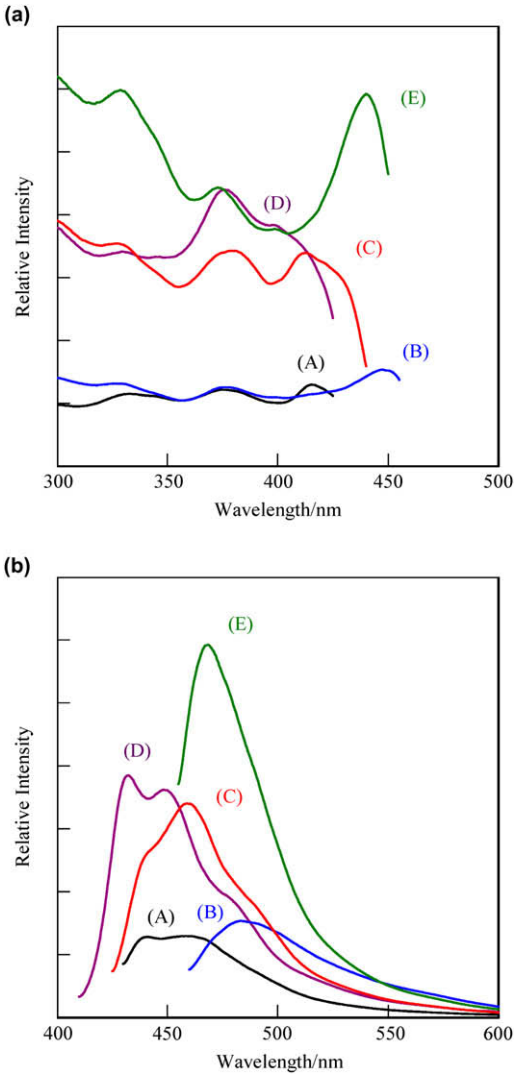

Figure 3. (a) Solid-state excitation and (b) fluorescence spectra of the guest-free and the guest-inclusion crystals of **1**; (A) **1** (guest-free): λ_{ex}=415 nm, λ_{em}=460 nm; (B) **1**·acetic acid: λ_{ex}=447 nm, λ_{em}=483 nm; (C) **1**·1-butanol: λ_{ex}=413 nm, λ_{em}=459 nm; (D) **1**·morpholine: λ_{ex}=398 nm, λ_{em}=432 nm; (E) **1**·propionic acid: λ_{ex}=440 nm, λ_{em}=469 nm.

2.5. Relation between the solid-state fluorescence properties and X-ray crystal structures of guest-inclusion compounds

To understand the enclathrated guest effects on the fluorescence properties of the crystal, the crystal structures of the acetic acid-, 1-butanol-, and morpholine-inclusion compounds of **1** have been determined by X-ray diffraction analysis.

The crystal of **1**·acetic acid (H/G=1:1) is made up by a hydrogen bonded cluster unit composed of two hosts and two acetic acid guests (Fig. 4a). The two hosts and two guests are alternately linked by four NH···O hydrogen bonds to form a centrosymmetric ring, in which the imidazole ring is protonated by the acetic acid proton (N(1)H(1)···O(1) angle=174°, N(1)···O(1) distance=2.609(3) Å and N(2)H(2)···O(2) angle=169°, N(2)···O(2) distance=2.767(3)) (Fig. 4b). Actually, the two bond lengths between two nitrogens (N(1) and N(2)) and C(15) in imidazole ring are 1.34 Å and 1.35 Å, respectively, which are nearly the same. There are two styles of π–π stacking overlap between host molecules. One is the π–π overlapping between the phenanthroimidazole and *p*-(diphenylamino)phenyl parts in the cluster unit (Fig. 4b: stacking I). The other is observed between the neighboring cluster units, where the phenanthrene ring parts are overlapping (Fig. 4c: stacking II). There are 15 and 22 short interatomic π–π contacts of less than 3.6 Å, and the average distance of the interatomic π–π contacts is ca. 3.48 Å and 3.54 Å, respectively, which suggest strong π–π interactions between the host molecules.

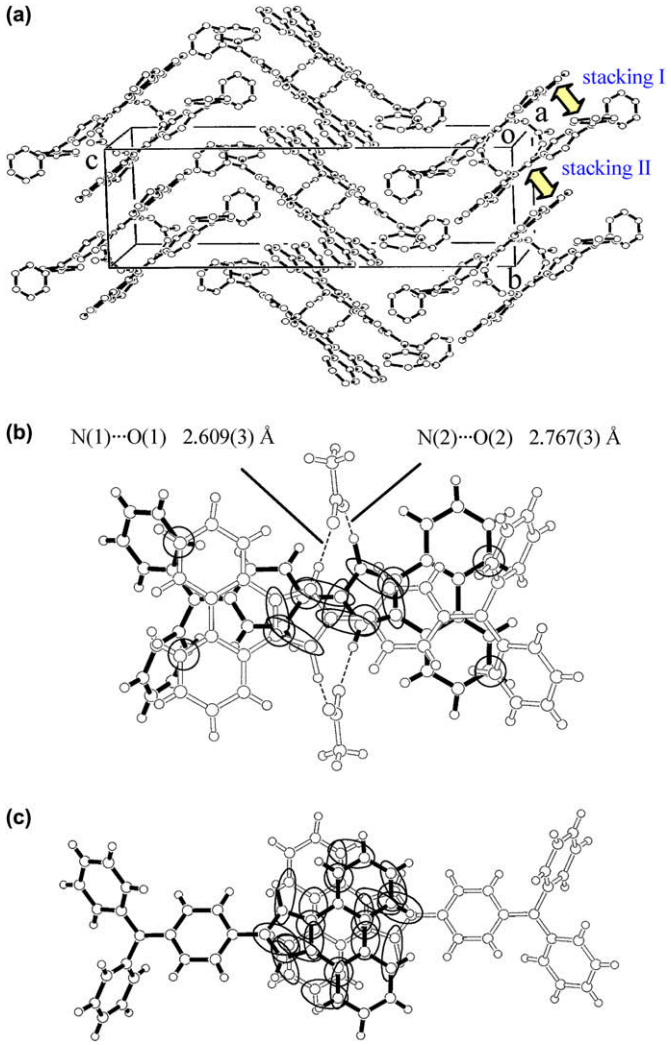

Figure 4. Crystal structure of **1**·acetic acid; (a) a stereoview of the molecular packing structure, (b) top view of a cluster unit (stacking I), and (c) a top view between two cluster units (stacking II). The circles represented in (b) and (c) show short interatomic π–π contacts of less than 3.6 Å.

Like the crystal of **1**·acetic acid, the crystal of **1**·1-butanol (H/G=1:1) is built up by the hydrogen bonded cluster unit composed of two hosts and two 1-butanol guests (Fig. 5a). However, although

the two hosts and two guests are alternately linked by four NH···O hydrogen bonds to form a centrosymmetric ring, the imidazole ring of the host is not protonated by the 1-butanol proton, in contrast to the crystal of **1**·acetic acid. As shown in Figure 5b, the proton of the imidazole ring of host is directing toward the oxygen of the guest (N(1)H(1)···O(1) angle=160(1)°, N(1)···O(1) distance=2.871(3) Å) and the hydroxyl proton of the guest is directing toward an imino nitrogen of another host (O(1)H(2)···N(2)* angle=166°, O(1)···N(2)* distance=2.899(3) Å). The bond lengths between two nitrogens (N(1) and N(2)) and C(15) in imidazole ring are 1.33 Å and 1.37 Å, respectively, showing that the differences between the two lengths are attributed to the C–N single bond and the C=N double bond of imidazole ring. Similar to the crystal of **1**·acetic acid, there are two styles of π–π stacking overlap between host molecules. In the π–π overlapping between the two hosts in the cluster unit (Fig. 5b: stacking I), there are 17 short interatomic π–π contacts of less than 3.6 Å, and the average distance of the interatomic π–π contacts is ca. 3.53 Å. On the other hand, the π–π overlapping of two hosts between the neighboring cluster units in **1**·1-butanol is smaller than that in **1**·acetic acid (Fig. 5c: stacking II); there are 7 short interatomic π–π contacts of less than 3.6 Å, and the average distance of the interatomic π–π contacts is ca. 3.47 Å, suggesting the reduction of the π–π interactions between the host molecules in comparison with the crystal of **1**·acetic acid.

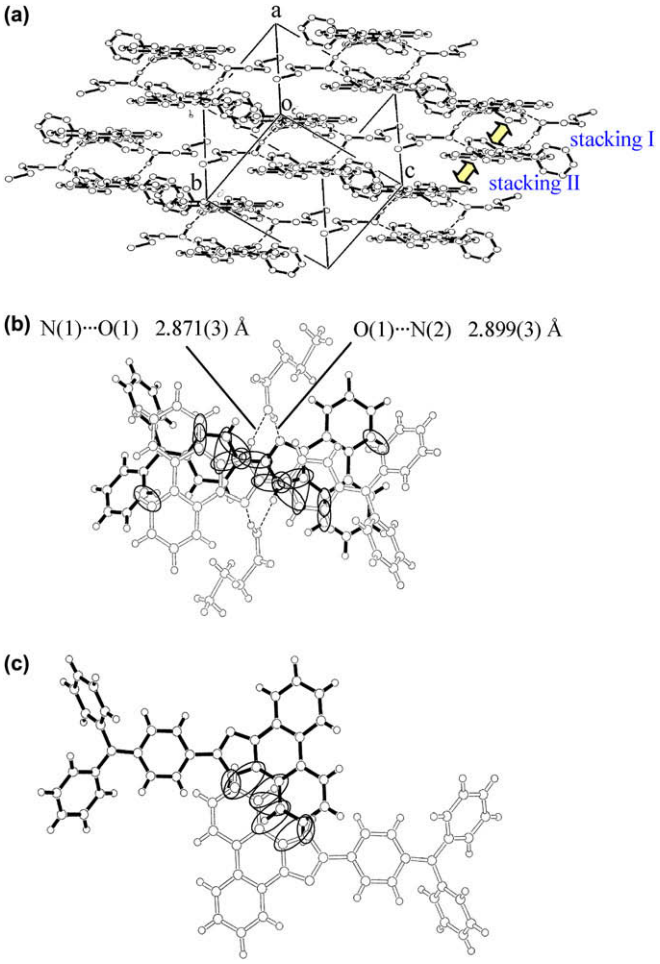

Figure 5. Crystal structure of **1**·1-butanol; (a) a stereoview of the molecular packing structure, (b) top view of a cluster unit (stacking I), and (c) a top view between two cluster units (stacking II). The circles represented in (b) and (c) show short interatomic π–π contacts of less than 3.6 Å.

In the crystal of **1**·morpholine (H/G/H_2O=2:1:2), there are two crystallographically independent host molecules (Fig. 6a). The crystal of **1**·morpholine is built up by the hydrogen bonded cluster unit composed of two crystallographically independent host molecules and two water molecules, in which the imidazole ring of the host is not protonated by the water molecule similar to the crystal of **1**·1-butanol. As shown in Figure 6b, in the cluster unit, the proton of the imidazole ring of host is directing toward the oxygen of the water molecule (N(1)H(1)···O(1) angle=166°, N(1)···O(1) distance=2.80(1) Å) and the hydroxyl proton of the water molecule is directing toward an imino nitrogen of another host (O(1)H(48)··· N(5) angle=172°, O(1)···N(5) distance=3.04(1) Å). Thus, similar to the crystal of **1**·1-butanol, the bond lengths between two nitrogens (N(1) and N(2)) and C(15) in imidazole ring are ca. 1.32 Å and ca. 1.37 Å, respectively. Interestingly, the morpholine molecule is linked by a hydrogen bond to two water molecules in order to connect the neighboring cluster units. Therefore, an continuous intermolecular hydrogen bonding chain of (···H···H_2O···G···H_2O···) is formed through two-type intermolecular hydrogen bonding between morpholine molecule and two water molecules and the above intermolecular hydrogen bonding between host and water molecule in cluster unit; the proton of water molecule is directing

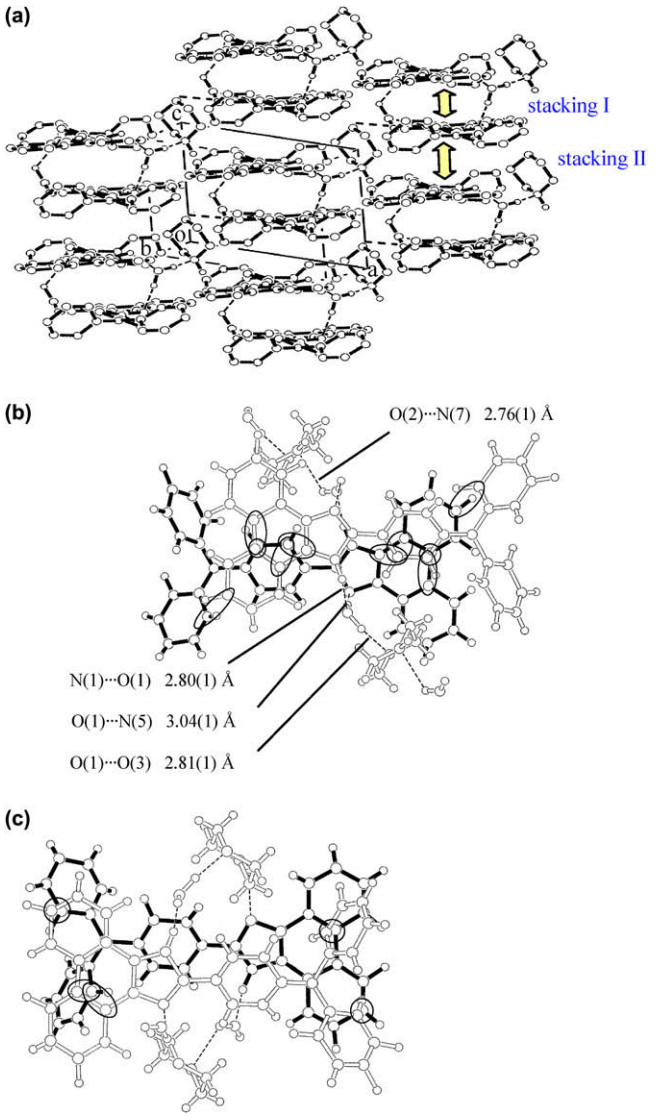

Figure 6. Crystal structure of **1**·morpholine with 2H_2O; (a) a stereoview of the molecular packing structure, (b) top view of a cluster unit (stacking I), and (c) a top view between two cluster units (stacking II). The circles represented in (b) and (c) show short interatomic π–π contacts of less than 3.6 Å.

toward the nitrogen of morpholine (O(2)H(49)···N(7) angle=119°, O(2)···N(7) distance=2.76(1) Å) and the proton of water molecule in another cluster unit is directing toward the oxygen of morpholine (O(1)H(47)···O(3) angle=171°, O(1)···O(3) distance=2.81(1) Å). There are two styles of π–π stacking overlap between host molecules. In the π–π overlapping between the two hosts in the cluster unit (Fig. 6b: stacking I), there are 10 short interatomic π–π contacts of less than 3.6 Å, and the average distance of the interatomic π–π contacts is ca. 3.53 Å. On the other hand, in the π–π overlapping of two host between the neighboring cluster units (Fig. 6c: stacking II), there are five short interatomic π–π contacts of less than 3.6 Å and the average distance of the interatomic π–π contacts is ca. 3.47 Å, suggesting the reduction of the π–π interactions between the host molecules in comparison with the crystals of **1**·acetic acid and **1**·1-butanol.

On the bases of the solid-state photophysical data and the crystal structures of the guest-inclusion compounds, we discuss the effects of the enclathrated guest on the solid-state photophysical properties of the clathrate compounds. So far, it has been clarified that strong intermolecular π–π interactions or continuous intermolecular hydrogen bonding between neighboring fluorophores induce the large red-shift of the absorption and fluorescence maxima and an intense fluorescence quenching in the solid state.[2–4,8] The wavelengths of the fluorescence excitation and emission maxima of guest-free crystal **1** are red-shifted by 50 nm and 59 nm compared with those of **1** in 1,4-dioxane, respectively. Unfortunately, although it is difficult to obtain sufficient sizes of single crystals for guest-free compound of **1** to carry out the X-ray structural analysis, the weak solid-state fluorescence intensity of guest-free crystal **1** is responsible for the above reasons. A comparison of the above three crystal structures shows that the strength of the π–π interactions between the fluorophores decrease in the following order: **1**·acetic acid->**1**·butanol>**1**·morpholine. These results confirm that the differences in the destruction of the host–host π–π interactions by enclathration of the guest molecules are reflected on the solid-state fluorescence intensity of the crystals. On the other hand, in our previous works,[3] we have demonstrated that continuous intermolecular hydrogen bonding between hosts (···H···H···) or an one-dimensional chain ranging alternately host and guest (···H···G···H···) is a principal factor of fluorescence quenching in the solid state, whereas the continuous intermolecular hydrogen bonding of (···H···G···G···) hardly contribute to quenching of the solid-state fluorescence. The intermolecular hydrogen bonding chain of (···H···H_2O···G···H_2O···) in the crystal of **1**·morpholine is similar to that of (···H···G···G···). Therefore, in the crystal of **1**·morpholine, the significant reductions of the π–π interactions between the host fluorophores by the enclathrated morpholine molecule are the main reason for the dramatic fluorescence enhancement and the blue-shift of the absorption and fluorescence maxima of the crystals. On the other hand, on the bases of the absorption and fluorescence spectra of **1** in acetic acid, the semi-empirical MO calculations and the X-ray crystal structure of **1**·acetic acid, the protonation of the imidazole ring of host **1** in the crystal of **1**·acetic acid and **1**·propionic acid would contribute to a red-shift of the absorption and emission spectra of the crystals because of an increase of intramolecular charge-transfer character of the host fluorophore by strong resonance interaction of the diphenylamino group with the protonated imidazole ring.

3. Conclusions

We have designed and synthesized a phenanthro[9,10-*d*]imidazole-type fluorescent clathrate host, 2-[4-(diphenylamino)-phenyl]-1*H*-phenanthro[9,10-*d*]imidazole (**1**) with imidazole ring and diphenylamino group. We found that the crystal of **1** exhibits fluorescence enhancement behavior with a blue-shift of the emission maximum upon enclathration of organic solvent molecules such as 1-butanol and morpholine, whereas the crystal of **1** exhibits fluorescence enhancement behavior with a red-shift of the emission maximum upon enclathration of carboxylic acid such as acetic acid and propionic acid. Our results indicated that the modulation of the solid-state fluorescence properties should be achieved by a combination of the fluorescent clathrate host and guest molecule; the electronic structure of fluorescent host in the solid state and the crystal structure are controlled by enclathration of the guests such as neutral, acidic, and basic molecules.

4. Experimental section

4.1. General procedure

Elemental analyses were measured with a Perkin Elmer 2400 II CHN analyzer. IR spectra were recorded on a JASCO FT/IR-5300 spectrophotometer for samples in KBr pellet form. Single-crystal X-ray diffraction was performed on Rigaku AFC7S diffractometer. Absorption spectra were observed with a JASCO U-best30 spectrophotometer and fluorescence spectra were measured with a JASCO FP-777 spectrophotometer. The fluorescence quantum yields (Φ) were determined by a Hamamatsu C9920-01 equipped with CCD by using a calibrated integrating sphere system (λ_{ex}=363 nm). For the measurement of the solid-state fluorescence excitation and emission spectra of the crystals, Jasco FP-1060 attachment was used. ^{1}H NMR spectra were recorded on a JNM-LA-400 (400 MHz) FT NMR spectrometer with tetramethylsilane (TMS) as an internal standard.

4.2. Synthesis of 2-[4-(diphenylamino)phenyl]-1*H*-phenanthro[9,10-*d*]imidazole (1)

A solution of 9,10-phenanthrenequinone (1.54 g, 7.42 mmol), *p*-diphenylaminobenzaldehyde (2.02 g, 7.40 mmol), and ammonium acetate (9.14 g, 0.12 mol) in acetic acid (70 ml) was stirred at 110 °C for 2 h. The reaction mixture was poured into ice-cold water. The resulting precipitate was filtered, washed with water, and dried. The residue was chromatographed on silica gel (CH_2Cl_2/ethyl acetate=10:1 as eluent) to give **1** (3.12 g, yield 91%) as an milk-white powder; mp 310–313 °C; ^{1}H NMR (400 MHz, DMSO-d_6, TMS) δ=7.10–7.14 (m, 8H), 7.35 (t, *J*=7.07 Hz, 4H), 7.61 (t, *J*=7.07 Hz, 2H), 7.71 (d, *J*=7.07 Hz, 2H), 8.18 (d, *J*=7.56 Hz, 2H), 8.53 (d, *J*=7.81 Hz, 2H), 8.84 (d, *J*=8.53 Hz, 2H), 7.54 (br, 1H, –NH); IR (KBr): ν=3083, 1591 cm^{-1}.Elemental analysis calcd (%) for $C_{25}H_{23}N_3$: C, 85.87; H, 5.02; N, 9.10. Found: C, 86.06; H, 5.18; N. 9.37.

4.3. Preparation of guest-inclusion crystals

The host compound **1** was dissolved with heating in respective guest–solvent. The solution was filtered and kept for a few days at room temperature. The crystals that formed were collected by filtration. The host (H)/guest (G) stoichiometric ratio of the inclusion compounds was determined by means of ^{1}H NMR integration and CHN analysis.

*4.3.1. Host **1** (guest-free).* The host **1** (300 mg) was dissolved by warming in acetonitrile (500 ml), and the resulting solution was allowed to stand at room temperature. The crystals (milk-white, needle, 120 mg) were collected and dried on the filter paper.

*4.3.2. Crystal **1**·acetic acid (H/G=1:1).* The host **1** (600 mg) was dissolved by warming in a mixture of acetic acid and acetonitrile (volume ratio of 1:10, 210 ml), and the resulting solution was allowed to stand at room temperature. The crystals (yellow, prism,

313 mg) were collected and dried on the filter paper. Elemental analysis calcd (%) for $C_{35}H_{27}N_3O_2$: C, 80.59; H, 5.34; N, 8.06. Found: C, 80.41; H, 5.22; N 8.13.

*4.3.3. Crystal **1**·propionic acid (H/G=1:2).* The host **1** (300 mg) was dissolved by warming in propionic acid (210 ml), and the resulting solution was allowed to stand at room temperature. The crystals (yellow, prism, 209 mg) were collected and dried on the filter paper. Elemental analysis calcd (%) for $C_{39}H_{35}N_3O_4$: C, 76.83; H, 5.79; N, 6.87. Found: C, 76.58; H, 5.74; N, 6.96.

*4.3.4. Crystal **1**·1-butanol (H/G=1:1).* The host **1** (600 mg) was dissolved by warming in 1-butanol (100 ml), and the resulting solution was allowed to stand at room temperature. The crystals (yellowish white, prism, 252 mg) were collected and dried on the filter paper. Elemental analysis calcd (%) for $C_{37}H_{33}N_3O$: C, 82.96; H, 6.21; N, 7.84. Found: C, 82.96; H, 6.30; N, 7.98.

*4.3.5. Crystal **1**·morpholine (H/G/H_2O=2:1:2) with 2H_2O.* The host **1** (300 mg) was dissolved by warming in a mixture of morpholine and water (volume ratio of 2:1, 300 ml), and the resulting solution was allowed to stand at room temperature. The crystals (white, prism, 141 mg) were collected and dried on the filter paper. Elemental analysis calcd (%) for $C_{70}H_{59}N_7O_3$: C, 80.36; H, 5.68; N, 9.37. Found: C, 80.34; H, 5.79; N, 9.47.

4.4. X-ray crystallographic studies

The reflection data were collected at 23±1 °C on a Rigaku AFC7S four-circle diffractometer by 2θ–ω scan technique, and using graphite-monochromated Mo Kα (λ=0.71069 Å) radiation at 50 kV and 30 mA. In all cases, the data were corrected for Lorentz and polarization effects. A correction for secondary extinction was applied. The reflection intensities were monitored by three standard reflections for every 150 reflections. An empirical absorption correction based on azimuthal scans of several reflections was applied. All calculations were performed using the teXsan[9] crystallographic software package of Molecular Structure Corporation. CCDC-740523 (**1**·acetic acid), CCDC-740524 (**1**·1-butanol), and CCDC-740525 (**1**·morpholine with 2H_2O) contain the supplementary crystallographic data for this paper. These data can be obtained free of charge from The Cambridge Crystallographic Data Centre via www.ccdc.cam.au.uk/data_request/cif.

*4.4.1. Crystal of **1**·acetic acid (H/G=1:1).* The transmission factors ranged from 0.99 to 1.00. The crystal structure was solved by direct methods using SIR 92.[10] The structures were expanded using Fourier techniques.[11] The non-hydrogen atoms were refined anisotropically. Some hydrogen atoms were refined isotropically, the rest were fixed geometrically and not refined. Crystallographic data: $C_{35}H_{27}N_3O_2$, M=521.62, monoclinic, a=10.92(1), b=10.050(3), c=25.180(3) Å, β=90.99(3)°, U=2761(2) Å^3, ρ_{calcd}=1.254 g cm^{-3}, T=296.2 K, space group $P2_1/n$ (no.14), Z=4, μ(Mo Kα)=0.79 cm^{-1}, 5123 reflections measured, 4853 unique (R_{int}=0.061), which were used in all calculations. The final R indices [$I>2\sigma(I)$], $R1$=0.050, $wR(F^2)$=0.161.

*4.4.2. Crystal of **1**·1-butanol (H/G=1:1).* The transmission factors ranged from 0.90 to 1.00. The crystal structure was solved by direct methods using SIR 92.[10] The structures were expanded using Fourier techniques.[11] The non-hydrogen atoms were refined anisotropically. Some hydrogen atoms were refined isotropically, the rest were fixed geometrically and not refined. Crystallographic data: $C_{37}H_{33}N_3O$, M=535.59, triclinic, a=10.688(4), b=13.987(7), c=10.027(2) Å, α=91.43(3)°, β=102.41(2)°, γ=91.89(3)°, U=1462.2 (8) Å^3, ρ_{calcd}=1.217 g cm^{-3}, T=296.2 K, space group $P\bar{1}$ (no. 2), Z=2, μ(Mo Kα)=0.73 cm^{-1}, 5444 reflections measured, 5145 unique (R_{int}=0.037), which were used in all calculations. The final R indices [$I>2\sigma(I)$], $R1$=0.063, $wR(F^2)$=0.163.

*4.4.3. Crystal of **1**·morpholine (H/G/H_2O=2:1:2) with 2H_2O.* The transmission factors ranged from 0.96 to 1.00. The crystal structure was solved by direct methods using SIR 92.[10] The structures were expanded using Fourier techniques.[11] The non-hydrogen atoms were refined anisotropically. Some hydrogen atoms were refined isotropically, the rest were fixed geometrically and not refined. Crystallographic data: $C_{70}H_{59}N_7O_3$, M=1046.28, triclinic, a=9.914(2), b=16.867(4), c=8.617(2) Å, α=103.48(2)°, β=100.49(2)°, γ=93.89 (2)°, U=1368.6(6) Å^3, ρ_{calcd}=1.269 g cm^{-3}, T=296.2 K, space group $P1$ (no.1), Z=2, μ(Mo Kα)=0.79 cm^{-1}, 5162 reflections measured, 4813 unique (R_{int}=0.041), which were used in all calculations. The final R indices [$I>2\sigma(I)$], $R1$=0.042, $wR(F^2)$=0.137.

4.5. Computational methods

The semi-empirical calculations were carried out with the WinMOPAC Ver. 3.9 package (Fujitsu, Chiba, Japan). Geometry calculations in the ground state were made using the AM1 method.[7] All geometries were completely optimized (keyword PRECISE) by the eigenvector following routine (keyword EF). Experimental absorption spectra of the eight compounds were compared with their absorption data by the semi-empirical method INDO/S (intermediate neglect of differential overlap/spectroscopic).[6] All CNDO/S calculations were performed using single excitation full SCF/CI (self-consistent field/configuration interaction), which includes the configuration with one electron excited from any occupied orbital to any unoccupied orbital, where 225 configurations were considered [keyword CI (15 15)].

Acknowledgements

This work was partially supported by a Grant-in-Aid for Science and Research from the Ministry of Education, Science, Sport and Culture of Japan (Grant 21550181) and by a Special Research Grant for Green Science from Kochi University.

References and notes

1. (a) Imai, Y.; Kawaguchi, K.; Harada, T.; Sato, T.; Ishikawa, M.; Fujiki, M.; Kuroda, R.; Matsubara, Y. *Tetrahedron Lett.* **2007**, *49*, 2927; (b) Imai, Y.; Murata, K.; Kawaguchi, K.; Sato, T.; Tajima, N.; Kuroda, R.; Matsubara, Y. *Chem. Asian J.* **2008**, *3*, 625.
2. (a) Yoshida, K.; Miyazaki, H.; Miura, Y.; Ooyama, Y.; Watanabe, S. *Chem. Lett.* **1999**, 837; (b) Yoshida, K.; Ooyama, Y.; Tanikawa, S.; Watanabe, S. *Chem. Lett.* **2000**, 714; (c) Yoshida, K.; Ooyama, Y.; Tanikawa, S.; Watanabe, S. *J. Chem. Soc., Perkin Trans. 2* **2002**, 708; (d) Ooyama, Y.; Yoshida, K. *New J. Chem.* **2005**, *29*, 1204; (e) Ooyama, Y.; Yoshida, K. *Eur. J. Org. Chem.* **2008**, *15*, 2564.
3. (a) Yoshida, K.; Uwada, K.; Kumaoka, H.; Bu, L.; Watanabe, S. *Chem. Lett.* **2001**, 808; (b) Ooyama, Y.; Nagano, S.; Okamura, M.; Yoshida, K. *Eur. J. Org. Chem.* **2008**, *35*, 5899; (c) Ooyama, Y.; Nagano, S.; Yoshida, K. *Tetrahedron* **2009**, *65*, 1467.
4. (a) Fei, Z.; Kocher, N.; Mohrschladt, C. J.; Ihmels, H.; Stalke, D. *Angew. Chem., Int. Ed.* **2003**, *42*, 783; (b) Scott, J. L.; Yamada, T.; Tanaka, K. *New J. Chem.* **2004**, *28*, 447.
5. (a) Mishra, A. K.; Dogra, S. K. *Bull. Chem. Soc. Jpn.* **1985**, *58*, 3587; (b) Dey, J.; Dogra, S. K. *J. Phys. Chem.* **1994**, *98*, 3638; (c) Krishnamoorthy, C.; Dogra, S. K. *J. Org. Chem.* **1999**, *64*, 6566.
6. (a) Ridley, J. E.; Zerner, M. C. *Theor. Chim. Acta* **1973**, *32*, 111; (b) Ridley, J. E.; Zerner, M. C. *Theor. Chim. Acta* **1976**, *42*, 223; (c) Bacon, A. D.; Zerner, M. C. *Theor. Chim. Acta* **1979**, *53*, 21; (d) Kurtz, H. A.; Stewart, J. J. P.; Dieter, D. M. *J. Comput. Chem.* **1990**, *11*, 82.
7. Dewar, M. J. S.; Zoebisch, E. G.; Healy, E. F.; Stewart, J. J. P. *J. Am. Chem. Soc.* **1985**, *107*, 3902.
8. (a) Langhals, H.; Potrawa, T.; Nöth, H.; Linti, G. *Angew. Chem., Int. Ed. Engl.* **1989**, *28*, 478; (b) Langhals, H.; Ismael, R.; Yürük, O. *Tetrahedron* **2001**, *56*, 5435; (c) Yoshida, K.; Ooyama, Y.; Miyazaki, H.; Watanabe, S. *J. Chem. Soc., Perkin Trans. 2* **2002**, 700; (d) Ooyama, Y.; Nakamura, T.; Yoshida, K. *New J. Chem.* **2005**, *29*, 447; (e) Ooyama, Y.; Okamoto, T.; Yamaguchi, T.; Suzuki, T.; Hayashi, A.; Yoshida, K. *Chem.—Eur. J.* **2006**, 7827; (f) Ooyama, Y.; Harima, Y. *Chem. Lett.* **2006**, 902; (g) Ooyama, Y.; Yoshikawa, S.; Watanabe, S.; Yoshida, K. *Org. Biomol. Chem.* **2006**, *4*, 3406; (h) Ooyama, Y.; Kagawa, Y.; Harima, Y. *Eur. J. Org. Chem.*

2007, *22*, 3613; (i) Ooyama, Y.; Mamura, T.; Yoshida, K. *Eur. J. Org. Chem.* **2007**, *30*, 5010; (j) Ooyama, Y.; Mamura, T.; Yoshida, K. *Tetrahedron Lett.* **2007**, *48*, 5791; (k) Ooyama, Y.; Yoshikawa, S.; Watanabe, S.; Yoshida, K. *Org. Biomol. Chem.* **2007**, *5*, 1260.

9. teXsan; Crystal Structure Analysis Package, Molecular Structure Corporation 1985 and 1992.
10. Altomare, A.; Burla, M. C.; Camalli, M.; Cascarano, M.; Giacovazzo, C.; Guagliardi, A.; Polidori, G. *J. Appl. Crystallogr.* **1994**, *27*, 435.
11. DIRDIF94 Beurskens, P. T.; Admiraal, G.; Beurskens, G.; Bosman, W. P.; de Gelder, R.; Israel, R.; Smits, J. M. M. *The DIRIF94 Program System, Technical Report of the Crystallography Laboratory*; University of Nijmegen: The Netherlands, 1994.